



OPEN

Arsenic album 30C exhibits crystalline nano structure of arsenic trioxide and modulates innate immune markers in murine macrophage cell lines

Suvasmita Rath^{1,2,6}, Jyoti Prava Jema^{2,6}, Kamali Kesavan³, Sagar Mallick³, Jyotsnarani Pradhan², Gagan Bihari Nityananda Chainy², Debadatta Nayak⁴, Subhash Kaushik⁴ & Jagneshwar Dandapat^{2,5}✉

Macrophages are associated with innate immune response and M1-polarized macrophages exhibit pro-inflammatory functions. Nanoparticles of natural or synthetic compounds are potential triggers of innate immunity. As_2O_3 is the major component of the homeopathic drug, Arsenic album 30C. This has been claimed to have immune-boosting activities, however, has not been validated experimentally. Here we elucidated the underlying mechanism of Ars. alb 30C-mediated immune priming in murine macrophage cell line. Transmission Electron Microscopy (TEM) and X-ray diffraction (XRD) used for the structural analysis of the drug reveals the presence of crystalline As_2O_3 nanoparticles of cubic structure. Similarly, signatures of M1-macrophage polarization were observed by surface enhanced Raman scattering (SERS) in RAW 264.7 cells with concomitant over expression of M1 cell surface marker, CD80 and transcription factor, NF- κ B, respectively. We also observed a significant increase in pro-inflammatory cytokines like iNOS, TNF- α , IL-6, and COX-2 expression with unaltered ROS and apoptosis in drug-treated cells. Enhanced expression of Toll-like receptors 3 and 7 were observed both in transcriptional and translational levels after the drug treatment. In sum, our findings for the first time indicated the presence of crystalline As_2O_3 cubic nanostructure in Ars. alb 30C which facilitates modulation of innate immunity by activating macrophage polarization.

Abbreviations

TLR	Toll like receptors
NF- κ B	Nuclear factor kappa-light-chain-enhancer of activated B cells (NF- κ B)
IL-6	Interleukin 6
HIF-1 α	Hypoxia-inducible factor 1 α
MyD88	Myeloid differentiation primary response 88
TRIF	TIR-domain-containing adaptor-inducing interferon- β
LPS	Lipopolysaccharides
SERS	Surface-enhanced Raman scattering
TEM	Transmission electron microscopy
PRRs	Pattern recognition receptors
TIR	Toll-interleukin-1 receptor
DMEM	Dulbecco's modified eagle medium
TNF- α	Tumor necrotic factor α

¹Centre of Environment, Climate Change and Public Health, Utkal University, Vani Vihar, Bhubaneswar, Odisha, India. ²Post Graduate Department of Biotechnology, Utkal University, Bhubaneswar, Odisha, India. ³CSIR-Institute of Minerals and Materials Technology, Bhubaneswar, Odisha, India. ⁴Central Council for Research in Homeopathy, New Delhi, India. ⁵Centre of Excellence in Integrated Omics and Computational Biology, Utkal University, Bhubaneswar, Odisha 751004, India. ⁶These authors contributed equally: Suvasmita Rath and Jyoti Prava Jema. ✉email: jd.biotech@utkaluniversity.ac.in; jdandapat.nou@gmail.com

SDS-PAGE	Sodium dodecyl sulfate polyacrylamide gel electrophoresis
PVDF	Polyvinylidene fluoride
DCFDA	Dichlorodihydrofluorescein diacetate
ROS	Reactive oxygen species
iNOS	Inducible nitric oxide synthase
SAED	Selected area electron diffraction
HR	High resolution
FFT	Fast Fourier transform
As ₂ O ₃	Arsenic trioxide
PAMPs	Pathogen-associated molecular patterns
NK	Natural killer
CMDNs	Cell-membrane derived nanoparticles
ANOVA	Analysis of variance
ssRNA	Single stranded ribonucleic acid
NP	Nanoparticle
TBST	Tris-buffered saline with 0.1% tween 20 detergent
NFDM	Non-fat dry milk
PBST	Phosphate buffered saline with tween 20

Innate immunity is the body's first line of defence against any pathogenic attack¹. Microbes and microbes-derived pathogenic factors are recognized and cleared by the action of innate immune effector molecules². Various cellular components of innate immune system include neutrophils, dendritic cells, eosinophils, Langerhans cells, macrophages, and Natural killer (NK) cells³. An array of cell surface receptors on these innate immune cells, also known as pattern recognition receptors (PRRs), enables them to detect pathogens or pathogen-associated molecular patterns (PAMPs)⁴. Toll-like receptors (TLRs) are major PRRs responsible for the detection of microbial signature molecules⁵. Among all TLRs, TLR-3 and TLR-7 are predominantly involved in antiviral immunity^{6,7}. TLR-3 recognizes double stranded RNA (dsRNA) molecules and exhibits antiviral host response by the production of type I interferons (IFNs), pro-inflammatory cytokines, and chemokines⁸. Toll-interleukin-1 receptor (TIR)-domain containing adaptor-inducing IFN- β (TRIF) is the adaptor molecule essential for TLR-3 function⁹. Similarly, TLR-7 recognizes single stranded RNA (ssRNA) molecules and executes its function through Myeloid differentiation primary response 88 (MyD88) adaptor protein¹⁰. TLR signalling induces the transcription factor NF- κ B, which further activates pro-inflammatory genes associated with M1 macrophage polarization¹¹. Elevated expressions of both TLR-3 and TLR-7 are evident in M1 polarized macrophages, which are associated with induced pro-inflammatory cytokine production^{12,13}.

The TLR signalling cascade is coupled with macrophage polarization and its phenotypic expression^{14,15}. Macrophages are active members of the innate immune system with impressive plasticity and potential for "differentiation into distinct phenotypes and functional attributes," commonly referred to as macrophage polarization. Such cellular responses to ambient stimuli under various pathophysiological conditions result in optimum and differential macrophage function^{16,17}. The tissue-resident macrophages (M0) are undifferentiated macrophages and precursors of polarized macrophages M1 and M2¹⁸. M1, or classically activated macrophages have pro-inflammatory activities, while M2, or alternatively activated macrophages have anti-inflammatory activities¹⁹. Activated macrophages are primed against pathogenic attacks; therefore, their activation plays a protective role in the pathogenesis of several inflammatory conditions²⁰. M1-polarized macrophages produce effector molecules such as reactive nitrogen intermediates and inflammatory cytokines, including IL-1 β , TNF- α , and IL-6, which act against pathogens by promoting immune responses^{20,21}.

TLR stimulation has also been linked to activation of adaptive immune response. Recent studies indicate the use of various TLR agonists like imiquimod, and CpG oligodeoxynucleotide (CpG ODN) as potential adjuvants during the design and development of COVID-19 vaccine. Further, some of the adjuvants have also been reported to induce a synergized effect comprising both adaptive and innate immunity^{22,23}. Several drugs and natural compounds are reported to have the ability to induce macrophage polarization, hence have significant therapeutic potential as immune modulators²⁴. Various preclinical studies demonstrate immunomodulatory, anti-oxidative, and therapeutic applications of naturally derived homeopathic drugs in a dose response manner^{25,26}. Arsenic album (Ars. alb) is a homeopathic drug prepared from arsenic trioxide and has a significant anticancer properties²⁵. It has been reported that Ars. alb ameliorates the toxic effect of arsenic trioxide in ultra-diluted form²⁷. Recently, Ars. alb 30C has also been reported to have preventive role against COVID-19 infection as evident from community-based and parallel cohort study in a contaminant zone of the Delhi region in India^{28,29}. Ye et al., demonstrated the immunomodulatory effect of trivalent arsenic, As (III) at a non-toxic concentration³⁰. Several other studies demonstrated the anticancer properties of As₂O₃ nanoparticles and their application in cancer immunotherapy^{31,32}. Although priming of innate immunity has been hypothesized behind the protective role of Ars. alb 30C described above, its function as an immune booster and detailed mechanism of its action is not been experimentally validated to date.

With this backdrop, the present study aims to underpin the possible causal mechanism of immunomodulation by Ars. alb 30C in RAW 264.7 macrophage cell line. Hypothesis of the study is that the immune priming potential of Ars. alb 30C is associated with the induction of innate immunity. Through our integrated experimental approaches, we have validated that Ars. alb 30C enhances innate immune signatures through upregulated expression of pro-inflammatory cytokines and concomitant polarization of M1 macrophages, as a part of its immune function. To gain insight into the mode of action of Ars. alb 30C, we have analysed its structure in Transmission Electron Microscope (TEM), X-ray diffraction (XRD) and M1 macrophage phenotype by Surface Enhanced

Raman Scattering (SERS). For the first time, we have reported the presence of arsenic trioxide nanoforms in *Ars. alb* 30C and correlated such nano structure behind its mechanism of immunomodulation. Our findings are in line with the previous reports which clearly supports nanostructure-driven innate immunity through macrophage polarization^{33,34}.

Therefore, the present study, with novel findings opens a new window to revisit *Ars. alb* 30C with different perspectives. Furthermore, this will provide hitherto unexplored opportunities and contribute to gaining its translational potential as a prospective alternative strategy for immune priming linked to several health consequences.

Results

Structural analysis with transmission electron microscopy (Fig. 1a–d) and X-ray diffraction (XRD) (supplementary Fig. S2)

Structural analysis of *Ars. alb* 30C was performed by transmission electron microscopy (TEM) and X-ray diffraction (XRD). Figure 1a, b showed the bright field low magnification TEM image of the ultra-high-diluted *Ars. alb* 30C sample and corresponding Selected Area Electron Diffraction (SAED) taken along [111] zone-axis. It clearly shows various planes such as $(2\bar{2}0)$, $(20\bar{2})$ and $(02\bar{2})$ planes that corresponds d-spacings of 0.466 nm of cubic As_2O_3 structure. Similarly, $(42\bar{2})$ and $(22\bar{4})$ planes correspond to 0.268 nm, while $(40\bar{4})$ and $(04\bar{2})$ planes

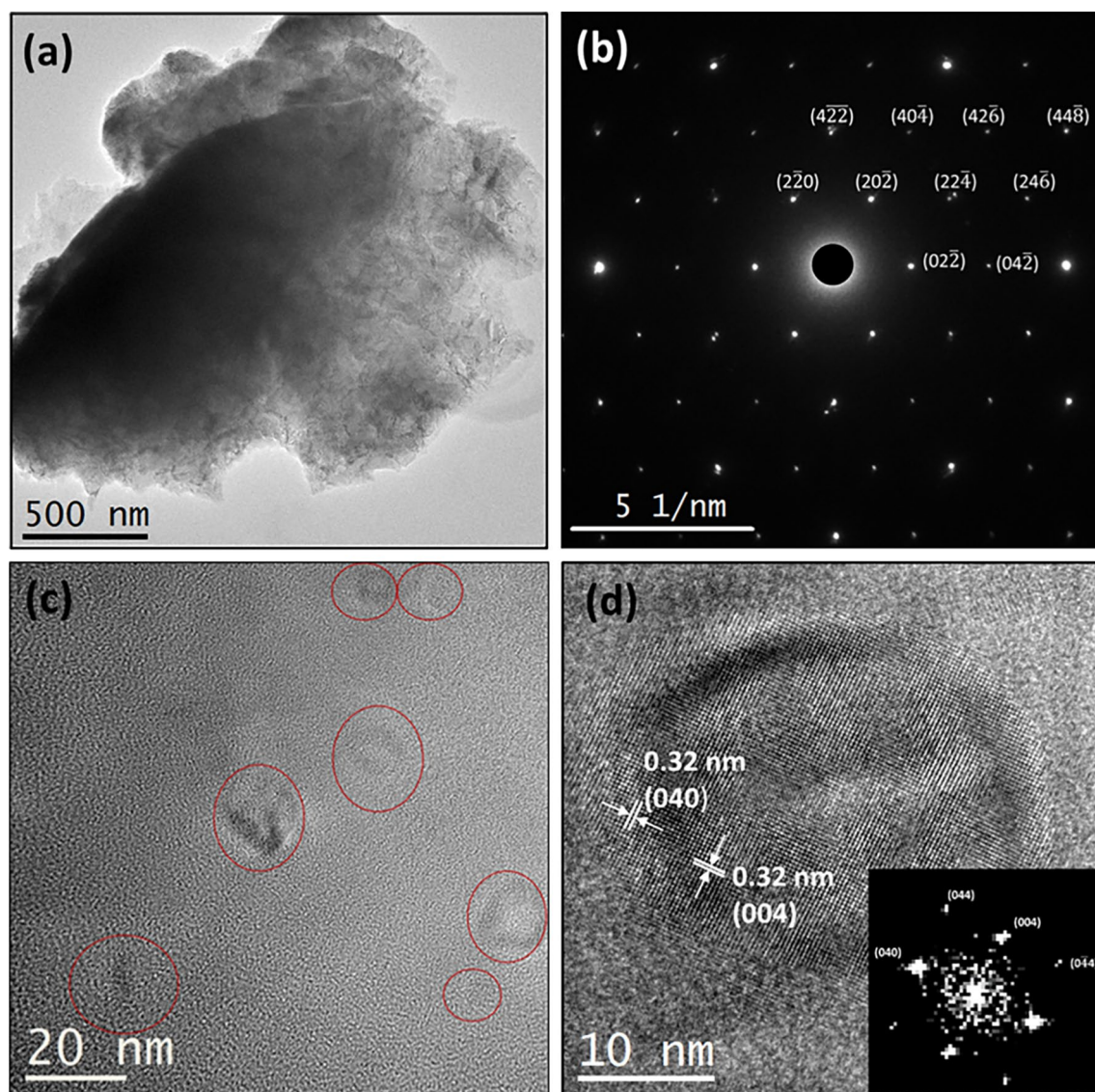


Figure 1. TEM analysis of *Ars. alb* 30C. **(a)** Low magnification bright field TEM image of the ultra-high-diluted *Ars. alb* 30C sample. **(b)** Selected area electron diffraction (SAED) taken along [111] zone-axis shows various planes corresponds to the d-spacings of 0.466 nm, 0.268 nm, and 0.176 nm of cubic As_2O_3 structure [JCPDS 00-002-1451]. **(c)** High-Resolution TEM (HRTEM) image of the sample indicates the formation of nanoparticles of average size ~ 15 nm. **(d)** HRTEM image of a single nano particle and corresponding fast Fourier transform (FFT) image (inset) clearly shows that the nanoparticles are highly crystalline in nature and various planes (along [100] zone-axis) confirms the presence of cubic As_2O_3 structure [JCPDS 00-002-1451].

correspond to 0.235 nm. Lastly, $(42\bar{6})$ and $(24\bar{6})$ planes correspond to 0.176 nm of cubic As_2O_3 structure [JCPDS 00-002-1451]. Figure 1c shows the High-Resolution TEM (HRTEM) image of the samples having nanoparticles. It indicates the formation of highly crystalline nanoparticles of an average size \sim of 15 nm. In Fig. 1d, the HRTEM image of a single nanoparticles and corresponding Fast Fourier Transform (FFT) image (inset) clearly shows that the nanoparticles are highly crystalline in nature and (040) (440) , (004) planes (along $[100]$ zone-axis) confirm the presence of cubic As_2O_3 structure [JCPDS 00-002-1451]. To further characterize, XRD scans were acquired from the drop-cast sample of Ars. alb 30C on 300 nm $SiO_2/Silicon$ substrate to investigate the crystallinity of As_2O_3 nanoparticles. In supplementary figure (Fig. S2), XRD pattern were analyzed, indexed and the peak position at 63.63° (2θ value) coincide with the (731) plane of As_2O_3 structure [Database: JCPDS 00-002-1451] Both TEM and XRD results confirmed the formation of highly crystalline nanoparticles of cubic As_2O_3 structure and their aggregates in the sample.

Macrophage polarization study by SERS (Fig. 2)

SERS is a phenomenon of enhancing Raman signal intensity using surface plasmonic nanoparticle substrate. Macrophage polarization states were evaluated by the SERS technique using gold plasmonic nanoparticles. RAW 264.7 cells were treated with Ars. alb 30C for 24 h or left untreated. 90% alcohol (10^{-4} dilution) was used as vehicle control. The spectral assignments³⁵ of Fig. 2 are depicted in Table 1. Macrophages were stimulated with Lipopolysaccharide (LPS) which acts as a positive control for M1 macrophage phenotype and the Raman spectra were evaluated in order to verify whether Raman spectroscopic analysis might distinguish M1-polarized macrophages from resting M0-macrophages upon activation with Ars. alb 30C. Comparing M0 and M1 spectra, the Raman bands around 910 cm^{-1} due to C-C stretching of amino acids of proteins and 1100 cm^{-1} due to lipid signatures undergoing major changes in peak intensity. Apart from these changes, there was neither the appearance nor disappearance of peaks. The other peaks exhibit small variations in the peak intensities. The

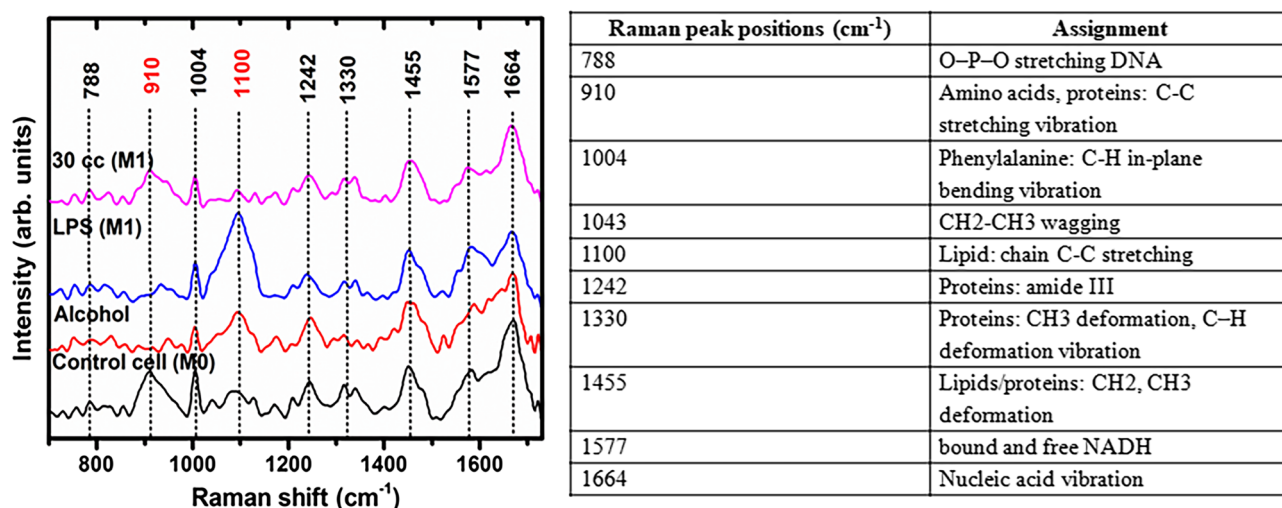


Figure 2. SERS fingerprint of M0 and M1-phenotype macrophages. SERS spectra represent the averages obtained from 20 cells for each group in the spectral range of $700\text{--}1800\text{ cm}^{-1}$. The peaks positions with red fonts indicate the positions where the largest spectral variations are found between M0 and M1 phenotypes.

Primers	Forward primer	Reverse primer	Annealing temperature ($^\circ\text{C}$)
TLR-3	5'-TCACTTGCTCATTCTCCCTT-3'	5'-GCCTGGCTAAGTTATTGTGC-3'	58
TLR-7	5'-TTCCTTCCGTAGGCTGAACC-3'	5'-GTAAGCTGGATGGCAGATCC-3'	58
TRIF	5'-CACGATCCTGCTCCTGACTG-3'	5'-CTGTGGAGCAGTCTGTTGT-3'	56
MyD88	5'-CATACCCTTGGTCGCGCTTA-3'	5'-CCAGGCATCCAACAACTGC-3'	56
NF- κ B	5'-CAGACCGCAGTATCCATAGC-3'	5'-CGTGAAGGGGTTATTGTTGG-3'	56
COX-2	5'-ACAACATCCCCTTCCTGCGA-3'	5'-TGGGCAGTCATCTGCTACGG-3'	58
iNOS	5'-TGAACCTTCTCAGCCACCTTGG-3'	5'-TGAAGAGAACTTCCAGGGGCA-3'	58
TNF- α	5'-TGCCTATGTCTCAGCCTCTT-3'	5'-GAGGCCATTTGGGAATTCT-3'	58
CD 80	5'-CCAAAGCATCTGAAGCTATGGC-3'	5'-TTCCAGCAATGACAGACAGC-3'	56
IRF3	5'-CGGAAAGAAGTGTTCGCGTTAGC-3'	5'-CAGGCTGCTTTTGCCATTGGTG-3'	58
GAPDH	5'-CAATGAATACGGCTACAGCAAC-3'	5'-AGGGAGATGCTCAGTGTGG-3'	58

Table 1. Sequences of forward primer and reverse primer used for real-time PCR.

spectrum corresponding to *Ars. alb* 30C matches with LPS-simulated macrophage spectrum. This confirms the M1 macrophage phenotype in *Ars. alb* 30C-treated cells.

Ars. alb 30C treatment is associated with unaltered ROS level and cell viability (Fig. 3a, b)

Total ROS level was measured by using DCFH-DA and no significant change in total ROS level was observed after *Ars. alb* 30C treatment as compared to vehicle control and media control cells (Fig. 3a). Further AO/PI double staining was performed to distinguish viable cells from dead cells by using fluorescence microscope. AO staining emits green fluorescence as it penetrates plasma membrane of viable cells. However, PI stains non-viable cells and emits red fluorescence. Our data showed uniform emission of green fluorescence with a healthy nucleus in control, alcohol, and *Ars. alb* 30C treated cells (Fig. 3b).

Induced expression of innate immune markers TLR-3, TLR-7, and their adaptor molecules in *Ars. alb* 30C-treated cells (Fig. 4a–h)

The present study aimed to validate the expression of innate immune markers TLR-3 and TLR-7 in *Ars. alb* 30C-treated cells both in transcript and translate levels. For this, RAW 264.7 cells were treated with *Ars. alb* 30C at a dilution of 10^{-4} along with 90% alcohol at a dilution of 10^{-4} as vehicle control and another group of cells left untreated for 24 h. Total RNA was isolated by TRIZOL method, and cDNA synthesis was performed using reverse transcriptase kit followed by real-time PCR. The RT-PCR data ($n = 3$) confirmed induced expression of TLR-3 and TLR-7 ($P \leq 0.05$) in transcript level after *Ars. alb* 30C treatment (Fig. 4a, b). We also observed induced expression of TLR-3 and TLR-7 adaptor molecules TRIF and MyD88, respectively in *Ars. alb* 30C-treated cells (Fig. 4c, d). As CD80 is used as M1 macrophage marker, we further investigated its expression in the transcript level by RT-PCR. Our data revealed induced expression of CD80 in *Ars. alb* 30C-treated cells as compared to vehicle control and media control cells (Fig. 4e).

RAW 264.7 cells were treated with *Ars. alb* 30C for 24 h. Protein samples were isolated and immunoblotting was performed to study the expression pattern of TLR-3 and TLR-7 protein levels. Representative western blot results ($n = 3$) showed that there is induced expression of TLR-3 and TLR-7 in *Ars. alb* 30C-treated cells as compared to the vehicle control and untreated cells (Fig. 4f, g). Induced MyD88 expression was validated in *Ars. alb* 30C-treated cells (Fig. 4h).

Confocal analysis for TLR-3 and TLR-7 expression (Fig. 5a, b)

To study the expression pattern of innate immune markers TLR-3 and TLR-7, we also performed confocal experiment by staining macrophage cells with TLR-3 and TLR-7 specific antibodies tagged with Alexa fluor 488. We observed induced expression of both TLR-3 and 7 in *Ars. alb* 30C-treated cells (Fig. 5a, b).

Up regulation of NF- κ B in *Ars. alb* 30C-treated RAW 264.7 cells (Fig. 6a, b)

As TLR signalling pathways activate downstream transcription factor NF- κ B, so we further validated expression of NF- κ B in transcript and translate levels. Our findings showed induced expression of NF- κ B in *Ars. alb* 30C-treated cells (Fig. 6a, b).

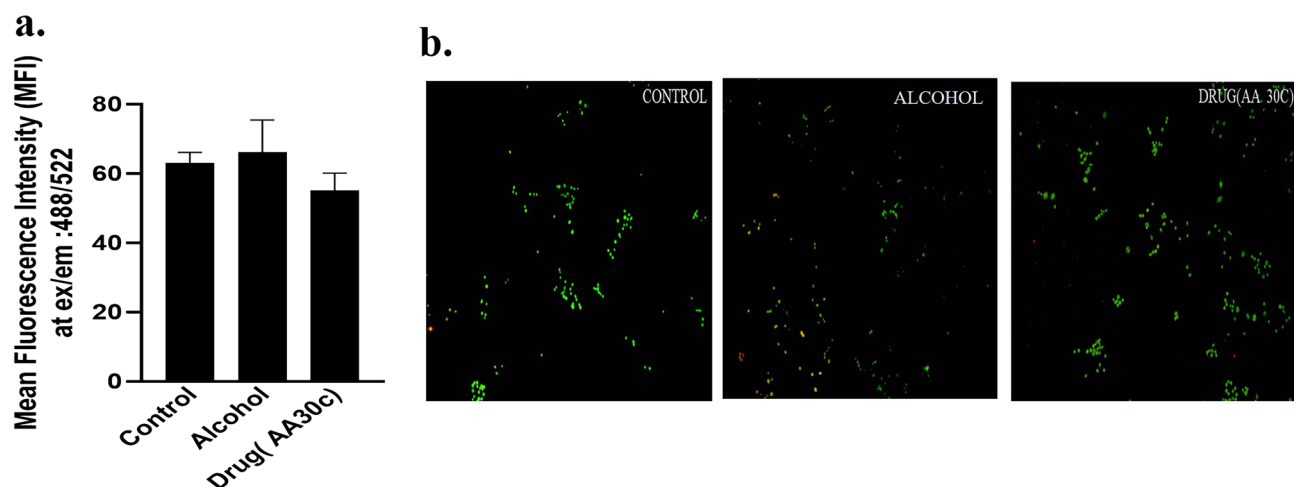


Figure 3. Measurement of total ROS level and microscopic detection of cell viability. **(a)** Total ROS level showing no significant change in *Ars. alb* 30C-treated cells as compared to the vehicle control and media control. Bars shown in panels represent normalized data (mean \pm SEM, $n = 3$), $*P \leq 0.05$. **(b)** Microscopic detection (magnification: $\times 10$) of apoptosis using AO/PI double staining in untreated, alcohol and *Ars. alb* 30C-treated RAW 264.7 cells.

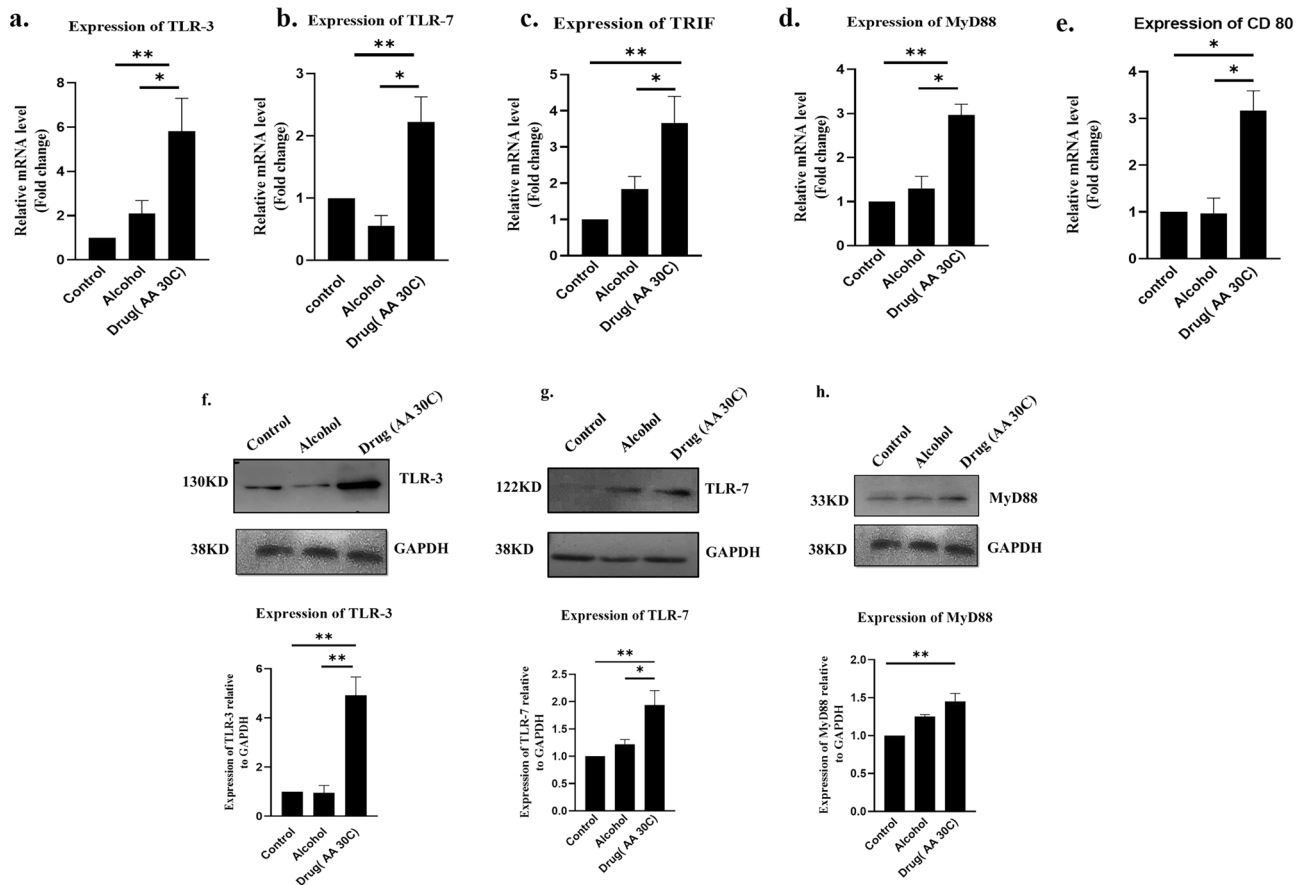


Figure 4. Expression of innate immune markers and downstream molecules in *Ars. alb* 30C-treated cells. (a–e) Real-time PCR showed induced TLR-3, TLR-7, TRIF, MyD88, and CD80 mRNA expression in *Ars. alb* 30C-treated cells as compared to the control samples. Bars shown in (a–e) represent normalized data (mean \pm SEM, $n = 3$), $*P \leq 0.05$. (f–h) Western blot analysis showed upregulation of TLR-3, TLR-7 & MyD88 in *Ars. alb* 30C-treated cell. Bars shown in (f–h) represent normalized data (mean \pm SEM, $n = 3$), $*P \leq 0.05$.

Induced expression of pro-inflammatory cytokines in *Ars. alb* 30C-treated cells (Fig. 7a–e)

Further, expression of pro-inflammatory cytokines TNF- α , COX-2, and iNOS at the transcript level was evaluated after *Ars. alb* 30C treatment. Our results confirmed the up regulation of these pro-inflammatory effector molecules in *Ars. alb* 30C-treated cells as compared to the untreated and alcohol-treated samples (Fig. 7a–c). The up-regulation of pro-inflammatory effector molecules like IL-6 and TNF- α after 30C treatment was confirmed by ELISA results (Fig. 7d. e).

Discussion

Research on nanoparticles (NPs) is a rapidly developing area of biomedicine and has made a significant contribution to health and the cure of diseases³⁶. The size, shape, and surface charge of NPs affect their cellular uptake and effectiveness³⁷. Due to larger surface area, a higher degree of surface charge, and proton exchangeability, nanoparticles show significant immunomodulatory activity^{38,39}. Various engineered and naturally-derived nanoparticles like cell membrane-derived nanoparticles (CMDNs) and silver nanoparticles (AgNPs), are reported to have immunomodulatory activity^{40,41}. Although, homeopathic drugs are prepared by ultrahigh dilutions; the possibility of formation of nanoparticles cannot be avoided^{42,43}. For the first time, we have reported the existence of crystalline As_2O_3 nanoparticles of cubic structure with an average size of ~ 15 nm and their aggregates in *Ars. alb* 30C by TEM & XRD. Our results are in line with previous findings of Ganeshchandra et al., who demonstrated widespread organ distribution of 15 nm gold NPs that signifies the effect of size on nanoparticle function⁴⁴. Based on the physicochemical properties and type of target cells, aggregates of NPs qualitatively influence their cellular uptake. Higher surface curvature, irregular shape, and asymmetric structure of the aggregates significantly affect their characteristics. This is the reason for the higher uptake of NPs aggregates rather than single NP⁴⁵. Nanoparticles can modulate the activity of innate immune cells by inducing inflammatory response⁴⁶. Several studies reported the ability of NPs to induce M0 to M1 macrophage polarization and reprogramming based on different physicochemical features, such as chemical composition, size, and surface modifications⁴⁷. Our SERS data indicated M1 macrophage polarization with a change in lipid and protein signatures like LPS-induced M1 macrophages⁴⁸. M1 macrophages are associated with TLR signalling pathways and induce the expression of pro-inflammatory effectors like TNF- α , COX-2, IL-6, and iNOS⁴⁹. TLR-3 and TLR-7 are markers of innate

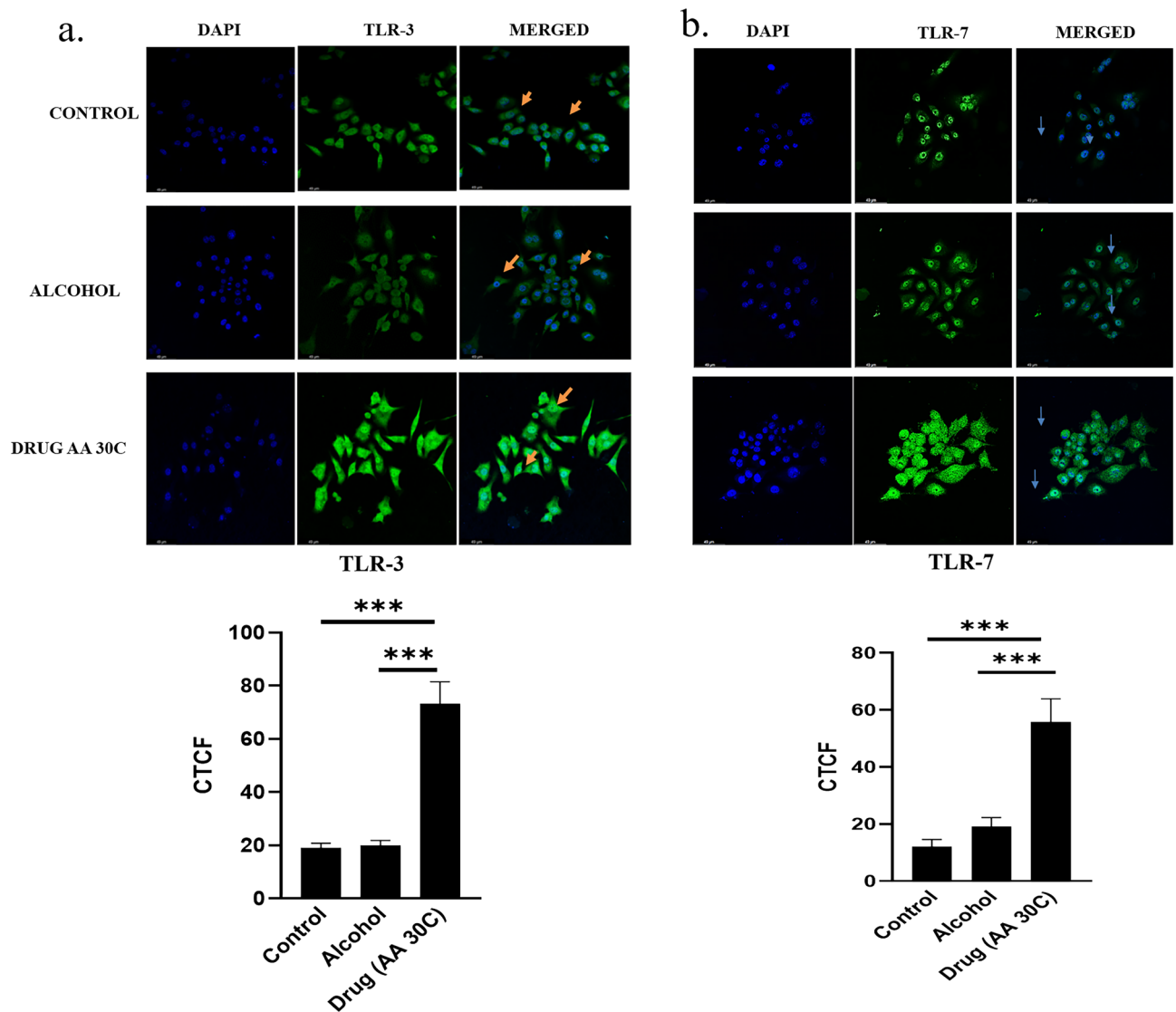


Figure 5. Confocal image analysis of *Ars. alb* 30C-treated RAW 264.7 cells. **(a)** Induced expression of TLR-3 was observed in *Ars. alb* 30C-treated cells as compared to control sample. Bars shown in panels represent normalized data (mean \pm SEM, $n = 3$), * $P \leq 0.05$. **(b)** Enhanced expression of TLR-7 observed in *Ars. alb* 30C-treated cells as compared to control samples. Bars shown in panels represent normalized data (mean \pm SEM, $n = 3$), * $P \leq 0.05$.

immune response expressed in the endosome of macrophage cells and are associated with pro-inflammatory pathways^{50,51}. TLR-3 responds to dsRNA and TLR-7 does the same against ssRNA^{52,53}. In this context recent reports confirmed the activation of TLR-3 and TLR-7 during SARS-CoV-2 infection⁵⁴. In a related study, Menezes et al., also demonstrated lower TLR-3 expression in patients having severe COVID-19 infections⁵⁵. Nayak et al., in their recent study demonstrated the significance of *Ars. alb* 30C as a preventive against SARS-CoV-2^{28,29}, but the underlying mechanism was not resolved. Our findings indicate induced expression of TLR-3 and TLR-7 in murine macrophages after *Ars. alb* 30C treatment along with their adaptor molecules TRIF and MyD88, respectively. This strongly supports the immunomodulatory potential of *Ars. alb* 30C and substantiates its preventive role against COVID-19 as proposed in previous studies^{28,29}. As TLR-3 and TLR-7 are mostly double-stranded and single-stranded RNA sensors, respectively, their induced expression might provide further antiviral responses in *Ars. alb* 30C-treated cells. It is essential to mention that several vaccines have been designed and developed taking TLR-3 and 7 agonists as adjuvants to improve the efficacy of the vaccines^{22,23}. We have further reported an unaltered total ROS level in *Ars. alb* 30C-treated cells, which suggests that the drug does not contribute to additional ROS production. No change in cell viability was observed after *Ars. alb* 30C treatment which indicated no significant cell death after drug treatment. Our findings are consistent with previous studies which also reported that *Ars. alb* 30C could promote antioxidant defence and upregulation of glutathione (GSH) with a concomitant reduction of total ROS level in yeast and mammals, which supports its therapeutic potential against oxidative stress-associated pathogenesis^{25,56,57}.

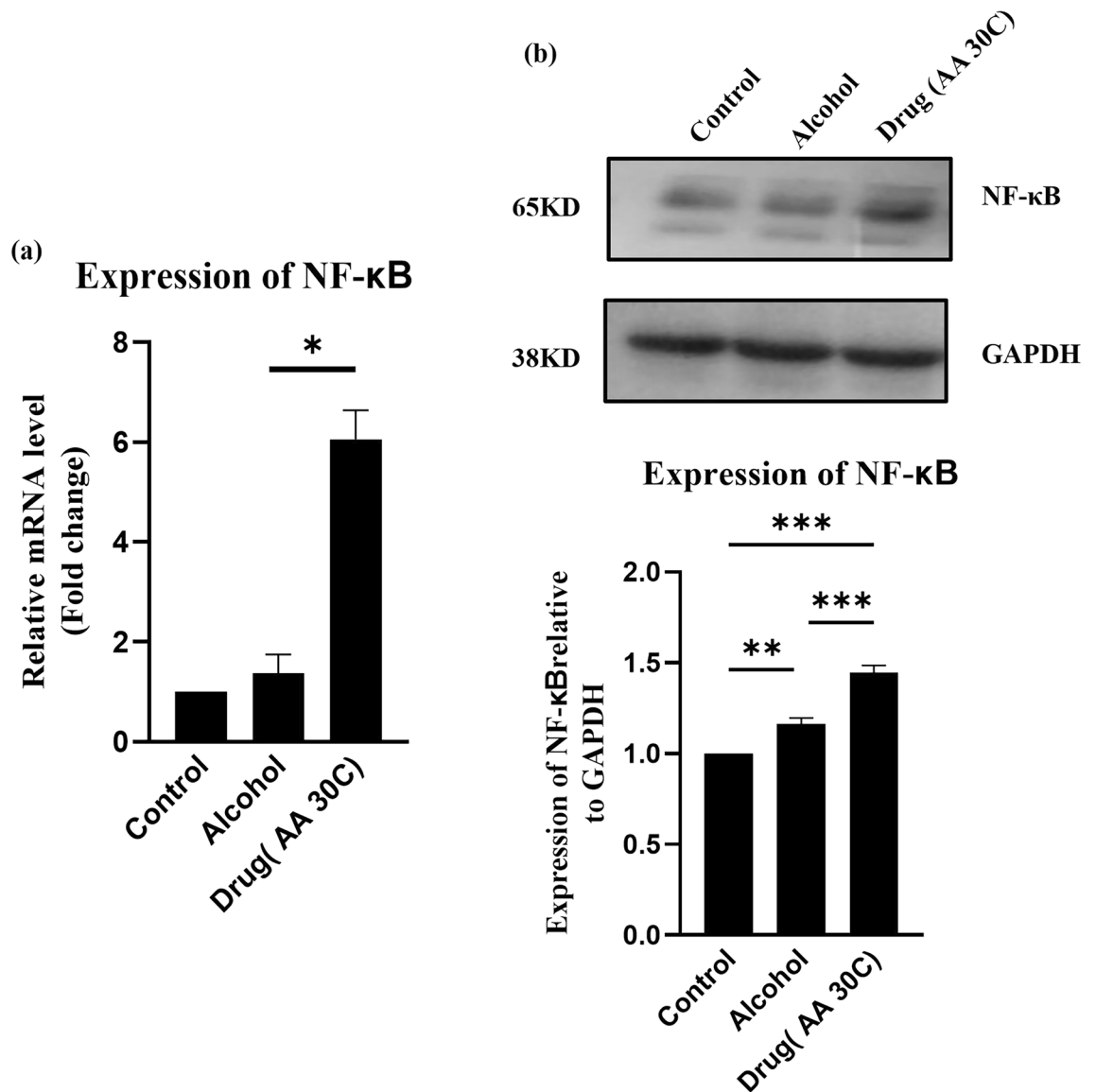


Figure 6. NF-κB expression in *Ars. alb.* 30C-treated cell. **(a,b)** Induced of expression NF-κB both at translational and transcript level was observed after *Ars. alb.* 30C treatment. Bars shown in panels represent normalized data (mean ± SEM, n = 3).

Taken together, this study, for the first time, reports the existence of a crystalline nanostructure of As_2O_3 in *Ars. alb.* 30C dilution, with a clear evidence of drug-dependent macrophage polarization, upregulation of TLR pathways, and a consequent immune effector function with distinct signature molecules. Figure 8 summarizes *Ars. alb.* 30C-mediated immune priming of macrophage and stimulation of “TLR-3-TRIF” & “TLR-7-MyD88”-signalling events leading to pro-inflammatory cytokine production as a part of its immune effector function.

Immunomodulation which promotes the innate protective mechanism or surveillance in the host, is increasingly receiving attention as an alternative to vaccination. This is due to the rapid and unpredictable mutation of microbial pathogens which can evade the immune barrier⁵⁸. An emerging strategy to combat infectious disease is the synergistic approach of vaccination and innate immune modulator (against TLR modulation). Mifsud et al., have opined that innate immune modulator-mediated long-term immunity is particularly important in cases of epidemic with recurrent infections. TLR stimulation by suitable agonist is crucial in sensing or detecting the pathogen/pathogen-derived signature molecule for their self-elimination⁵⁸. This work, using in vitro model, established the mechanism of action of *Ars. alb.* 30C as an immunomodulator. For the first-time our findings revealed the presence of As_2O_3 crystalline nanostructures in *Ars. alb.* 30C, providing compelling evidence to explain the causal mechanism. Furthermore, the expression of innate immune markers and pro-inflammatory cytokines related to M1 macrophages is evident in *Ars. alb.* 30C-treated murine macrophage cells.

As homeopathic drugs are less costly and have minimal side-effects, *Ars. alb.* 30C can be a prospective alternative medicine to boost innate immunity, with significant clinical applications. However, a major challenge to the acceptance of homeopathic medications is the lack of pharmacological validation. In this context, our findings provide considerable evidence in support of its efficacy and reveal a novel mechanism of *Ars. alb.* 30C-mediated

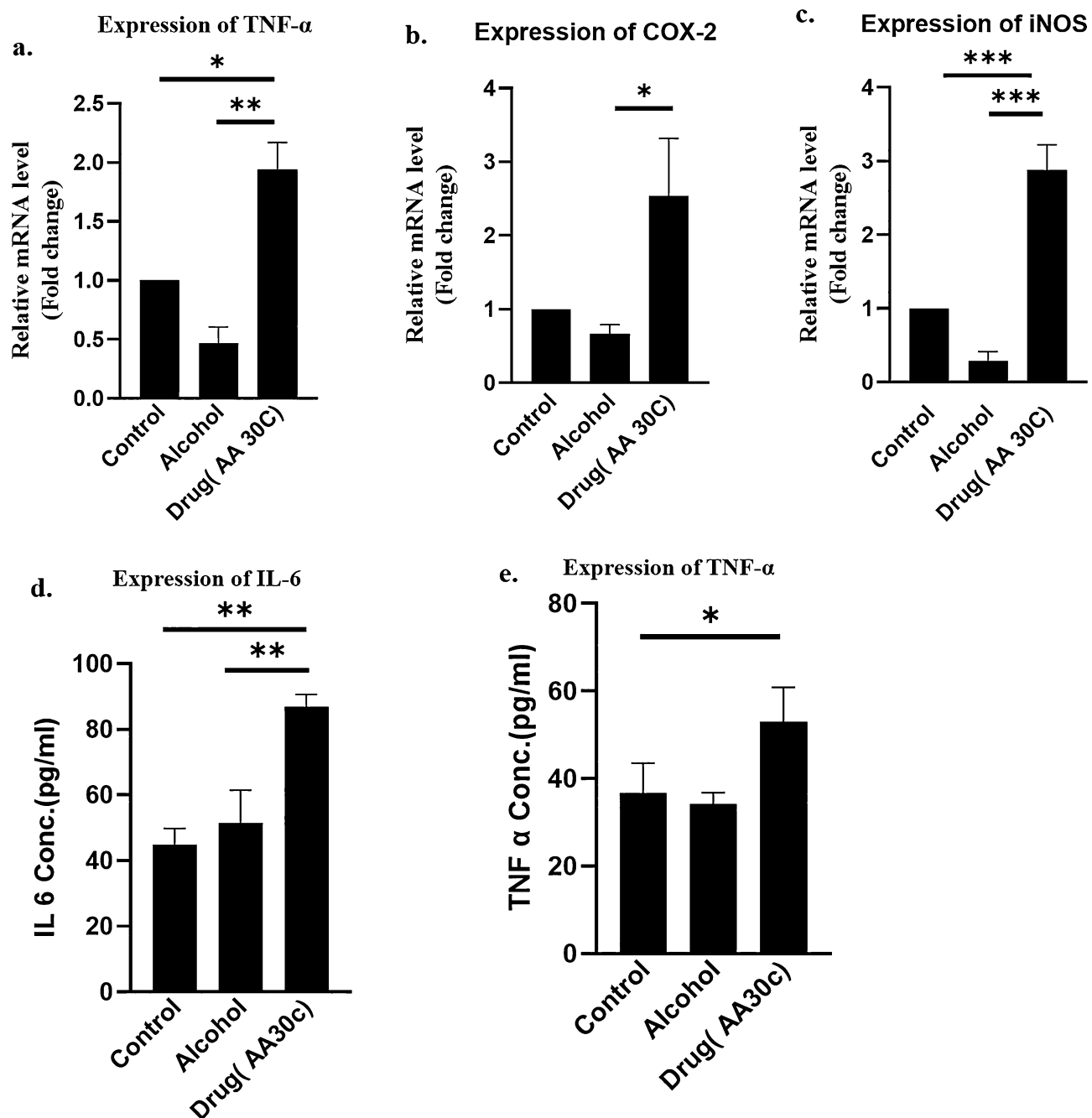


Figure 7. Expression of pro-inflammatory markers in *Ars. alb* 30C-treated cell. (a–c) Pro-inflammatory molecules like iNOS, COX-2, and TNF- α induced at transcript level after *Ars. alb* 30C treatment. Bars shown in panels represent normalized data (mean \pm SEM, n = 3), *P \leq 0.05. (d,e) Induced expression of IL-6 & TNF- α was observed in *Ars. alb* 30C-treated cells by ELISA. Bars shown in panels represent normalized data (mean \pm SEM, n = 3), *P \leq 0.05.

M1 macrophage polarization and induction of innate immune response. *Ars. alb* 30C can be used as innate immune modulator, particularly as TLR-3 and TLR-7 agonist, which can provide host-dependent long lasting innate immunity in general, and against the invading pathogens or infectious diseases, in particular. Nevertheless, further study with animal models and human trials needs to be carried out before translational intervention.

Materials and methods

Cell culture and *Ars. Alb* 30C treatment

Murine macrophage cell lines RAW 264.7 were obtained from National Centre for Cell Science (NCCS), Pune, India and cultured in DMEM complete medium under standard cell culture conditions⁵⁹. *Ars. alb* 30C was procured from Dr. Reckeweg.co, Germany and was used at a dilution of 10^{-4} with complete media by serial dilution.

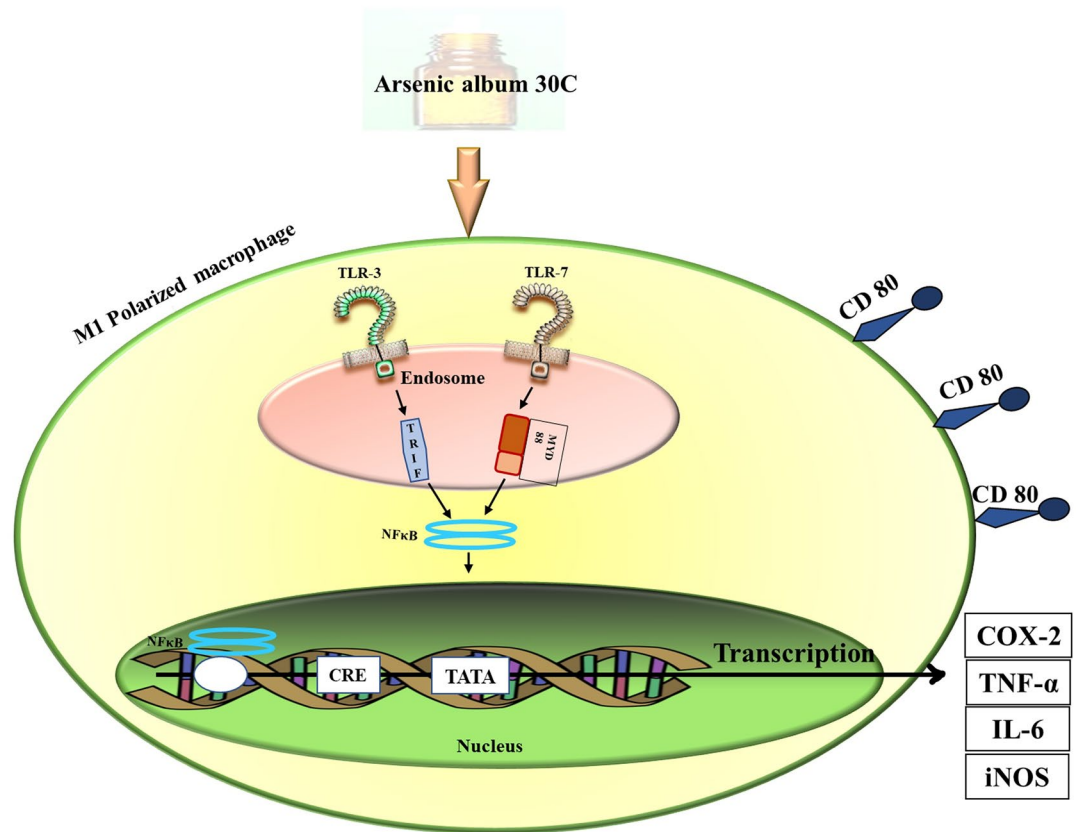


Figure 8. Proposed mechanism for Arsenic album 30C-induced M1-macrophage polarization and innate immune response. Arsenic album 30C crystalline nanostructure induces TLR-3 and TLR-7 expression in endosome of M1-polarized macrophage cells along with the adaptor molecules TRIF and MyD88 respectively, and surface marker CD80. Further, this activates transcription factor NF- κ B and downstream pro-inflammatory cytokines COX-2, TNF- α , IL-6, and iNOS.

Treatment was done for 24 h as per the standardised protocol. Since the drug was prepared in alcohol (90% ethanol), we included a solvent control (SC) as 90% ethanol which was also diluted to 10^{-4} with complete media⁶⁰.

Total RNA extraction and cDNA synthesis

1×10^6 RAW 264.7 cells were treated with Arsenic album 30C for 24 h and total RNA was extracted from treated, vehicle control and media control samples by using TRIZOL reagent (Invitrogen) according to the manufacturer's manual. Then the total RNA was reverse transcribed to synthesize cDNA using reverse transcriptase Revert Aid H minus (Thermo Scientific, USA). cDNA templates were diluted to 100 ng of working concentration.

Quantitative real-time PCR analysis

Real-time PCR was performed by using specific primers for TLR-3, TLR-7 and their adaptor molecules TRIF and MyD88, respectively. M1-associated transcription factor NF- κ B was also evaluated by real-time PCR. Expressions of pro-inflammatory effector molecules like COX-2, iNOS, and TNF- α were also checked for validation of M1-macrophage polarization. GAPDH was used as housekeeping gene (Table 1 for primer sequence). SYBR Green (ABI, USA) was used to amplify and detect DNA in qPCR by Quant studio 5 system (Applied Biosystems, CA, and USA). Real-time PCR amplification reactions were carried out in a final volume of 12.5 μ l, which contained 8.5 μ l dH₂O, 2.5 μ l SYBR Green, 0.5 μ l of each primer and 0.5 μ l diluted cDNA template. PCR conditions were as follows Hold stage: 50 °C for 2 min, 95 °C for 10 min, PCR stage: 95 °C for 15 s followed by suitable annealing for 1 min and 72 °C for 30 s.

SDS PAGE and western blotting

1×10^6 cells were seeded in each well of 60 mm cell culture plate and treated with Arsenic album 30C and 90% ethanol (10^{-4} diluted) as vehicle control. After 24 h of post-treatment, total proteins were isolated and estimated by Bradford's method⁶¹. 30 μ g of proteins were loaded in each well and separated by sodium dodecyl sulfate–polyacrylamide gel electrophoresis (SDS-PAGE) with a stacking gel concentration of 5% and a resolving gel concentration of 10%. The gel was run for 90 min at 45 milliamps, till the dye front moved out of the gel. Then, Western blotting was performed and the proteins were transferred (through wet transfer) to a polyvinylidene fluoride (PVDF) membrane using at 40 V for 4 h. After completion of transfer, membranes were incubated with blocking solution of 5% Non-Fat Dry milk (NFDm) in Tris-buffered saline with 0.1% Tween 20 detergent (TBST) buffer

for 1 h. Further, membranes were probed with specific antibodies against target molecules like TLR-7, TLR-3, MyD88, and NF- κ B (Santacruz, USA) at a dilution of 1:1000 in TBST for overnight at 4 °C. GAPDH (Imgenex India Pvt. Ltd., India) was used as a loading control at a dilution of 1:1000. Next day, blots were washed three times with 1 \times TBST followed by incubation with secondary antibodies (anti-rabbit and anti-mouse) at a dilution of 1:5000 in TBST for 1 h at room temperature, followed by another round of washing with 1 \times TBST and final wash with 1 \times TBS. ImmunoCruz western blotting luminol reagent (Santacruz, USA) was used as a detection reagent and developed using X-ray film. Images were scanned with a gel documentation system (VILBER, USA). Band intensity was quantified by using Image J densitometry software. GAPDH was used as an internal loading control to normalize the expression of the proteins. All the original blots referenced in the document are provided in the supplementary file.

Enzyme-linked immunosorbent assay (ELISA)

25 \times 10³ cells were seeded in each well of 96 well plates and Ars. alb 30C treatment was done along with vehicle control and media control. After 24 h of post-treatment cell supernatant were collected from all three groups, centrifuged at 1000 \times g at 4 °C for 20 min and the concentrations of TNF- α and IL-6 were measured with ELISA kits (Elabscience, USA) as per manufacturer's instruction. All samples were assayed in triplicate and measured at 450 nm wavelength.

Confocal microscopy

1 \times 10³ RAW 264.7 cells were seeded on 18 mm cover slips and treated with Ars. alb 30C for 24 h. Another group of cells were treated with 90% alcohol (10⁻⁴ diluted) and the third group was left untreated. After the incubation period was over, cells were fixed with 4% paraformaldehyde at 37 °C for 15 min followed by permeabilization with 0.1% Triton-X-100 for 15 min. Cells were washed with 1X Phosphate Buffered Saline with Tween 20 (PBST) for 3 times followed by blocking with 3% BSA for 1 h at room temperature. Then, primary antibodies were added specific for TLR-3 and TLR-7 at a dilution of 1:200 in 3% BSA for overnight at 4 °C. The next day, cells were washed with 1X PBST and incubated with fluorescently conjugated (Alexa fluor 488) secondary antibodies at a dilution of 1:1000 in blocking solution for 1 h in dark. Subsequently 3 times washing was performed with 1X PBST followed by treatment with nuclear stain DAPI (4', 6-Diamidino-2-Phenylindole, Dilactate) (Invitrogen) for 20 min at a dilution of 1:2000 in 1X PBS. Finally, coverslips were washed with 1 \times PBS for three times and mounted over slides by using Fluoromount aqueous mounting medium (Sigma Aldrich). Once the slides were dried, expression of TLR-3 and TLR-7 were assessed by a laser scanning confocal microscope (Confocal Microscope Platforms, Leica, STELLARIS). All images were acquired at room temperature and digitally processed along with intensity measurement by image J software.

Total reactive oxygen species (ROS) measurement

Total reactive oxygen species measurement was evaluated by Dichlorodihydrofluorescein diacetate (DCFH-DA) treatment as per standardized protocol⁶². Ars. alb 30C treated cells, 90% alcohol (10⁻⁴ diluted)-treated cells and control cells were treated with DCFH-DA for 1 h followed by PBS wash three times. Then, cells were sonicated for 2–3 min followed by centrifugation at 10,000 \times g for 5 min. Then supernatant was collected and fluorescence reading (Cary Eclipse Fluorescence Spectrophotometer, Agilent Technologies, USA) was taken at 488 nm excitation and 522 nm emission.

Acridine orange (AO) and propidium iodide (PI) double staining for cell viability

Cell viability and apoptosis induction in Ars. Alb 30C-treated cells was evaluated by PI and AO double staining assay⁶³ by using a fluorescent microscope (BX53, Olympus, Japan). RAW 264.7 cells were seeded at a density of 5 \times 10³ cells/ml on cover slips in a six well plate and treated with Ars. alb 30C for 24 h. Another group of cells were treated with 90% alcohol (10⁻⁴ diluted) and the third group was left untreated. After the incubation period cells were washed with 1 \times PBS and treated with 10 μ M of AO and 5 μ M of PI for 30 min. The stained cells were visualized under fluorescence microscope.

Surface-enhanced Raman scattering (SERS)

Macrophage polarization was detected using surface enhanced Raman spectroscopy (SERS) technique. 1 \times 10³ RAW 264.7 cells were seeded on cover slips and treated with Ars. alb 30C for 24 h. Lippopolysaccharide (LPS) (100 ng/ml) treated cells were used as a positive control for macrophage polarization from M0 to M1. The rest of the two groups were treated with 90% alcohol (10⁻⁴ dilution) and left untreated. Plasmonic gold nanoparticles of 15 nm size were used for surface enhancement. After incubation for 24 h, cover slips with cells were fixed using cold methanol (to reduce the fluorescence background)⁶⁴. Then gold nanoparticles were added to the cells and kept in the open air for 24 h. SERS spectra were obtained using a Renishaw Raman spectrometer coupled to an Olympus microscope and equipped with a 532 nm laser-focused on the cells' nucleus through a 100 \times objective (NA = 0.9). The same objective lens was used to collect Raman scattered light after interaction with the sample in backscattering geometry. The Raman peak positions were calibrated by the 520 cm⁻¹ vibrational band of a silicon wafer. Under similar conditions, 20 cell spectra for each stimulated group (M0, and M1) were measured in the spectral range of 700–1800 cm⁻¹. In order to minimize laser-induced heating of the specimens, low-power irradiation at the sample surface was used, approximately 3 mW, over a short exposure time (5 s laser exposure for 5 accumulations). The diffraction grating used had 2400 lines/mm, which yielded a spectral resolution of 1.5 cm⁻¹.

Data pre-processing and spectral analysis

Before conducting the spectral analysis, the spectra were smoothed, background-corrected, and normalized by the area to suppress external noise and enhance useful information about the biochemical composition of cells. All procedures were performed using Origin Lab software. The background spectra are subtracted from cellular spectra, ensuring that the measured signal is assigned only to the cells.

Transmission electron microscope

Transmission electron microscopy (TEM) was performed to evaluate the structural arrangement of Ars. alb 30C. The sample was transferred to a carbon-coated Cu-TEM grids and left to dry before observation. TEM investigation was performed on a JEOL-JEM-F-200 TEM operated at 200 kV.

X-ray diffraction (XRD)

To characterize the crystal structure, powder XRD diffraction ($\theta - 2\theta$) scans were recorded for the drop-coated films of Ars. alb 30C sample on 300 nm SiO₂/Silicon substrate, using Bruker DA VINCI D8 ADVANCE diffractometer equipped with a Cu-K α source ($\lambda = 0.154$ nm).

Statistics

Statistical analyses were performed using GraphPad Prism (GraphPad Software, San Diego, California, USA). The statistical significance among groups were determined using analysis of variance (ANOVA). All data are presented as mean \pm standard error of the mean (SEM) from three or more independent experiments. The level of significance was set at $p \leq 0.05$.

Data availability

The raw scanned blot images used in the figures are provided in Supplementary Data as supplementary Fig. 1. Other datasets used and/ or analysed in the current study are available from the corresponding author upon request.

Received: 1 June 2023; Accepted: 3 January 2024

Published online: 07 January 2024

References

- Marshall, J. S., Warrington, R., Watson, W. & Kim, H. L. An introduction to immunology and immunopathology. *Allergy Asthma Clin. Immunol.* **14**, 1–10 (2018).
- Bikard, D. & Marraffini, L. A. Innate and adaptive immunity in bacteria: mechanisms of programmed genetic variation to fight bacteriophages. *Curr. Opin. Immunol.* **24**, 15–20 (2012).
- Li, M. O. *et al.* Innate immune cells in the tumor microenvironment. *Cancer Cell* **39**, 725–729 (2021).
- Uthaisangsook, S., Day, N. K., Bahna, S. L., Good, R. A. & Haraguchi, S. Innate immunity and its role against infections. *Ann. Allergy Asthma Immunol.* **88**, 253–265 (2002).
- Fitzgerald, K. A. & Kagan, J. C. Toll-like receptors and the control of immunity. *Cell* **180**, 1044–1066 (2020).
- Matsumoto, M., Oshiumi, H. & Seya, T. Antiviral responses induced by the TLR3 pathway. *Rev. Med. Virol.* **21**, 67–77 (2011).
- O'Neill, L. A. TLR-7 and antiviral immunity. *Trends Immunol.* **23**, 234 (2002).
- Su, R. *et al.* The TLR3/IRF1/type III IFN axis facilitates antiviral responses against enterovirus infections in the intestine. *MBio* **11**, 22 (2020).
- Chen, Y., Lin, J., Zhao, Y., Ma, X. & Yi, H. Toll-like receptor 3 (TLR3) regulation mechanisms and roles in antiviral innate immune responses. *J. Zhejiang Univ. B* **22**, 609–632 (2021).
- Pal, A., Pal, A. & Baviskar, P. RIGI, TLR7, and TLR3 genes were predicted to have immune response against avian influenza in indigenous ducks. *Front. Mol. Biosci.* **8**, 633283 (2021).
- Ma, B. *et al.* Modular bioinformatics analysis demonstrates that a Toll-like receptor signaling pathway is involved in the regulation of macrophage polarization. *Mol. Med. Rep.* <https://doi.org/10.3892/mmr.2018.9486> (2018).
- Lu, C. H. *et al.* Involvement of M1 macrophage polarization in endosomal Toll-like receptors activated psoriatic inflammation. *Mediators Inflamm.* **2018**, 3523 (2018).
- Vidyarthi, A. *et al.* TLR-3 stimulation skews M2 macrophages to M1 through IFN- α signaling and restricts tumor progression. *Front. Immunol.* **9**, 1650 (2018).
- Koo, J., Hayashi, M., Verneris, M. R. & Lee-Sherick, A. B. Targeting tumor-associated macrophages in the pediatric sarcoma tumor microenvironment. *Front. Oncol.* **10**, 1–19 (2020).
- Meng, L. *et al.* Toll-like receptor 3 upregulation in macrophages participates in the initiation and maintenance of pristane-induced arthritis in rats. *Arthritis Res. Ther.* **12**, 103 (2010).
- Kishore, A. & Petrek, M. Roles of macrophage polarization and macrophage-derived miRNAs in pulmonary fibrosis. *Front. Immunol.* **12**, 6784 (2021).
- Twigg, H. Macrophages in innate and acquired immunity. *Semin. Respir. Crit. Care Med.* **25**, 21–31 (2004).
- Zhang, Y., Zou, J. & Chen, R. An M0 macrophage-related prognostic model for hepatocellular carcinoma. *BMC Cancer* **22**, 791 (2022).
- Cendrowicz, E., Sas, Z., Bremer, E. & Rygiel, T. P. The role of macrophages in cancer development and therapy. *Cancers (Basel)* **13**, 1946 (2021).
- Glass, C. K. & Natoli, G. Molecular control of activation and priming in macrophages. *Nat. Immunol.* **17**, 26–33 (2016).
- Mosser, D. M. & Edwards, J. P. Exploring the full spectrum of macrophage activation. *Nat. Rev. Immunol.* **8**, 958–969 (2008).
- Angelopoulou, A. *et al.* Imiquimod—A toll like receptor 7 agonist—Is an ideal option for management of COVID 19. *Environ. Res.* **188**, 109858 (2020).
- Liang, Z. *et al.* Adjuvants for coronavirus vaccines. *Front. Immunol.* **11**, 589833 (2020).
- Wang, Y., Smith, W., Hao, D., He, B. & Kong, L. M1 and M2 macrophage polarization and potentially therapeutic naturally occurring compounds. *Int. Immunopharmacol.* **70**, 459–466 (2019).
- Paumier, A., Verre, J., Tribolo, S. & Boujedaini, N. Anti-oxidant effect of high dilutions of *Arnica montana*, *Arsenicum Album*, and *Lachesis Mutus* in microglial cells in vitro. *Dose-Response* **20**, 155932582211036 (2022).

26. Gupta, V. & Mathur, M. Immunomodulatory effects of homeopathic medicines: A review of pre-clinical studies. *Indian J. Res. Homeopath.* **12**, 90 (2018).
27. Iye, E. C., Couchman, I. M. S. & Reddy, L. Therapeutic effect of arsenicum album on leukocytes. *Int. J. Mol. Sci.* **13**, 3979–3987 (2012).
28. Nayak, D. *et al.* Efficacy of *Arsenicum album* 30C in the prevention of COVID-19 in individuals residing in containment areas—A prospective, multicentre, cluster-randomized, parallel arm, community based, open-label study. *Complement. Med. Res.* <https://doi.org/10.1159/000526897> (2022).
29. Nayak, D. *et al.* Effectiveness of *Arsenicum album* 30C in prevention of COVID-19 in individuals residing in containment zones of Delhi—A prospective, community-based, parallel cohort study. *Homeopathy* <https://doi.org/10.1055/s-0042-1745755> (2022).
30. Ye, Y., Gaugler, B., Mohty, M. & Malard, F. Old dog, new trick: Trivalent arsenic as an immunomodulatory drug. *Br. J. Pharmacol.* **177**, 2199–2214 (2020).
31. Hu, J. *et al.* Local delivery of arsenic trioxide nanoparticles for hepatocellular carcinoma treatment. *Signal Transduct. Target. Ther.* **4**, 1–7 (2019).
32. Jadhav, V., Ray, P., Sachdeva, G. & Bhatt, P. Biocompatible arsenic trioxide nanoparticles induce cell cycle arrest by p21WAF1/CIP1 expression via epigenetic remodeling in LNCaP and PC3 cell lines. *Life Sci.* **148**, 41–52 (2016).
33. Zanganeh, S. *et al.* Iron oxide nanoparticles inhibit tumour growth by inducing pro-inflammatory macrophage polarization in tumour tissues. *Nat. Nanotechnol.* **11**, 986–994 (2016).
34. Italiani, P., Della Camera, G. & Boraschi, D. Induction of innate immune memory by engineered nanoparticles in monocytes/macrophages: From hypothesis to reality. *Front. Immunol.* **11**, 566309 (2020).
35. Ribeiro, A. R. B. *et al.* Application of Raman spectroscopy for characterization of the functional polarization of macrophages into M1 and M2 cells. *Spectrochim. Acta Part Mol. Biomol. Spectrosc.* **265**, 120328 (2022).
36. Salata, O. V. Applications of nanoparticles in biology and medicine. *J. Nanobiotechnol.* **6**, 1–6 (2004).
37. Kiio, T. M. & Park, S. Physical properties of nanoparticles do matter. *J. Pharm. Invest.* **51**, 35–51 (2021).
38. Li, Z., Liu, Y., Fang, X. & Shu, Z. Nanomaterials enhance the immunomodulatory effect of molecular targeted therapy. *Int. J. Nanomed.* **16**, 1631–1661 (2021).
39. Jang, J., Lim, D.-H. & Choi, I.-H. The impact of nanomaterials in immune system. *Immune Netw.* **10**, 85 (2010).
40. Yang, Y., Wang, K., Pan, Y., Rao, L. & Luo, G. Engineered cell membrane-derived nanoparticles in immune modulation. *Adv. Sci.* **8**, 1–20 (2021).
41. Alsaleh, N. B. *et al.* Silver nanoparticle immunomodulatory potential in absence of direct cytotoxicity in RAW 264.7 macrophages and MPRO 2.1 neutrophils. *J. Immunotoxicol.* **16**, 63–73 (2019).
42. Chikramane, P. S., Suresh, A. K., Bellare, J. R. & Kane, S. G. Extreme homeopathic dilutions retain starting materials: A nanoparticulate perspective. *Homeopathy* **99**, 231–242 (2010).
43. Vargheese, W. V. *Characterization of Arsenic Trioxide Nanoparticles in Ultra-Dilutions of Arsenicum Album at 12c, 30c and 200c Strengths Using Raman Spectroscopy Technique Introduction* (2021).
44. Sonavane, G., Tomoda, K. & Makino, K. Biodistribution of colloidal gold nanoparticles after intravenous administration: Effect of particle size. *Colloids Surf. B Biointerfaces* **66**, 274–280 (2008).
45. Behzadi, S. *et al.* Cellular uptake of nanoparticles: Journey inside the cell. *Chem. Soc. Rev.* **46**, 4218–4244 (2017).
46. Swartzwelder, B. J. *et al.* The impact of nanoparticles on innate immune activation by live bacteria. *Int. J. Mol. Sci.* **21**, 9695 (2020).
47. Boraschi, D. *et al.* Nanoparticles and innate immunity: New perspectives on host defence. *Semin. Immunol.* **34**, 33–51 (2017).
48. Orecchioni, M., Ghosheh, Y., Pramod, A. B. & Ley, K. Macrophage polarization: Different gene signatures in M1(LPS+) vs. classically and M2(LPS-) vs alternatively activated macrophages. *Front. Immunol.* **10**, 1084 (2019).
49. Yunna, C., Mengru, H., Lei, W. & Weidong, C. Macrophage M1/M2 polarization. *Eur. J. Pharmacol.* **877**, 173090 (2020).
50. Krieg, A. M. & Vollmer, J. Toll-like receptors 7, 8, and 9: linking innate immunity to autoimmunity. *Immunol. Rev.* **220**, 251–269 (2007).
51. Hu, Y. *et al.* Synergy of TLR3 and 7 ligands significantly enhances function of DCs to present inactivated PRRSV antigen through TRIF/MyD88-NF- κ B signaling pathway. *Sci. Rep.* **6**, 1–15 (2016).
52. Crozat, K. & Beutler, B. TLR7: A new sensor of viral infection. *Proc. Natl. Acad. Sci. USA* **101**, 6835–6836 (2004).
53. Tengroth, L. *et al.* Functional effects of Toll-like receptor (TLR)3, 7, 9, RIG-I and MDA-5 stimulation in nasal epithelial cells. *PLoS One* **9**, 3–10 (2014).
54. Bortolotti, D. *et al.* TLR3 and TLR7 RNA sensor activation during SARS-CoV-2 infection. *Microorganisms* **9**, 1820 (2021).
55. Menezes, M. C. S. *et al.* Lower peripheral blood Toll-like receptor 3 expression is associated with an unfavorable outcome in severe COVID-19 patients. *Sci. Rep.* **11**, 15223 (2021).
56. De, A. Potentized homeopathic drug Arsenicum Album 30C inhibits intracellular reactive oxygen species generation and up-regulates expression of arsenic resistance gene in arsenite-exposed bacteria *Escherichia coli*. *J. Chinese Integr. Med.* **10**, 210–227 (2012).
57. Das, D. Potentized homeopathic drug Arsenicum Album 30C positively modulates protein biomarkers and gene expressions in *Saccharomyces cerevisiae* exposed to arsenate. *J. Chinese Integr. Med.* **9**, 752–760 (2011).
58. Mifsud, E. J., Tan, A. C. L. & Jackson, D. C. TLR agonists as modulators of the innate immune response and their potential as agents against infectious disease. *Front. Immunol.* **5**, 79 (2014).
59. Taciak, B. *et al.* Evaluation of phenotypic and functional stability of RAW 264.7 cell line through serial passages. *PLoS One* **13**, 1–13 (2018).
60. Arora, S., Aggarwal, A., Singla, P., Jyoti, S. & Tandon, S. Anti-proliferative effects of homeopathic medicines on human kidney, colon and breast cancer cells. *Homeopathy* **102**, 274–282 (2013).
61. Bradford, M. A rapid and sensitive method for the quantitation of microgram quantities of protein utilizing the principle of protein-dye binding. *Anal. Biochem.* **72**, 248–254 (1976).
62. Kim, H. & Xue, X. Detection of total reactive oxygen species in adherent cells by 2',7'-dichlorodihydrofluorescein diacetate staining. *J. Vis. Exp.* **2020**, 1–5 (2020).
63. Bank, H. L. Assessment of islet cell viability using fluorescent dyes. *Diabetologia* **30**, 812 (1987).
64. Pissuwan, D. & Hattori, Y. Detection of adhesion molecules on inflamed macrophages at early-stage using SERS probe gold nanorods. *Nano-Micro Lett.* **9**, 1–9 (2017).

Acknowledgements

Authors would like to thank Central Council for Research in Homeopathy, CCRH, Ministry of AYUSH, Government of India for a collaborative research grant and supporting open access publication. SR thankful to the RUSA 2.0 Centre of Excellence (CoE) in Environment, Climate Change and Public Health (ECCPH), Utkal University supported by MHRD, Govt of India for the provisional fellowship. Support from DBT, Government of India, New Delhi to Department of Biotechnology, Utkal University and Center of Excellence in Integrated Omics and Computational Biology (under WB-OHEPEE), Utkal University, Bhubaneswar are also gratefully acknowledged for infrastructure support. We are thankful to Dr. Ashutosh Rath, senior scientist, CSIR-IMMT,

Bhubaneswar for analysis of TEM data and fruitful discussions. Our sincere gratitude to Dr. Soma Chattopadhyay, Scientist F, Institute of Life science, Bhubaneswar, for providing us Phospo-IRF and IRF antibodies. We are sincerely grateful to Dr. S. Deepika, Assistant Professor, Dept. of English, Utkal University, Bhubaneswar, for language correction and copy editing of this manuscript.

Author contributions

J.D., conceptualized, discussed, drafted, and revised the manuscript. S.R., conceptualized, discussed, performed experiments, drafted, and revised the manuscript. J.P.J., discussed, performed experiments, analysed data, and participated in manuscript writing. K.K., performed SERS and participated in manuscript writing. S.M., performed TEM. J.P., conducted experiments and analysing data, G.B.N.C., discussed and participated in manuscript writing. D.N., and S.K., revised the manuscript. All authors have read and agreed to the published version of the manuscript. All authors read and approved the final manuscript.

Funding

This work is supported by Central Council for Research in Homeopathy (CCRH), Ministry of AYUSH, Government of India (17-6/2015-16/CCRH/Tech/Coll/Utkal University/1762).

Competing interests

The authors declare no competing interests.

Additional information

Supplementary Information The online version contains supplementary material available at <https://doi.org/10.1038/s41598-024-51319-w>.

Correspondence and requests for materials should be addressed to J.D.

Reprints and permissions information is available at www.nature.com/reprints.

Publisher's note Springer Nature remains neutral with regard to jurisdictional claims in published maps and institutional affiliations.



Open Access This article is licensed under a Creative Commons Attribution 4.0 International License, which permits use, sharing, adaptation, distribution and reproduction in any medium or format, as long as you give appropriate credit to the original author(s) and the source, provide a link to the Creative Commons licence, and indicate if changes were made. The images or other third party material in this article are included in the article's Creative Commons licence, unless indicated otherwise in a credit line to the material. If material is not included in the article's Creative Commons licence and your intended use is not permitted by statutory regulation or exceeds the permitted use, you will need to obtain permission directly from the copyright holder. To view a copy of this licence, visit <http://creativecommons.org/licenses/by/4.0/>.

© The Author(s) 2024